

Multichannel matching pursuit and EEG inverse solutions

Piotr J. Durka ^{a,1}, Artur Matysiak ^{a,1},
Eduardo Martínez Montes ^b, Pedro Valdés Sosa ^b,
Katarzyna J. Blinowska ^{a,1}

^a*Department of Biomedical Physics, Institute of Experimental Physics, Warsaw University, ul. Hoża 69, 00-681 Warszawa, Poland, <http://brain.fuw.edu.pl>.*

^b*Cuban Neuroscience Center, Ave 25 #15202 esquina 158 Cubanacan, Playa, Area Code 11600, Habana, Cuba.*

Corresponding author: Piotr J. Durka, Warsaw University,
Institute of Experimental Physics, Department of Biomedical Physics,
ul. Hoża 69, 00-681 Warszawa, Poland. Email: durka@fuw.edu.pl,
tel. (48 22) 5532126, fax (48 22) 6226154

Abstract

We present a new approach to the preprocessing of the electroencephalographic time series for EEG inverse solutions. As the first step, EEG recordings are decomposed by multichannel matching pursuit algorithm—in this study we introduce a computationally efficient, suboptimal solution. Then, based upon the parameters of the waveforms fitted to the EEG (frequency, amplitude and duration), we choose those corresponding to the phenomena of interest, like e.g. sleep spindles. For each structure, the corresponding weights of each channel define a topographic signature, which can be subject to an inverse solution procedure, like e.g. Loreta, used in this work.

As an example, we present an automatic detection and parameterization of sleep spindles, appearing in overnight polysomnographic recordings. Inverse solutions obtained for single sleep spindles are coherent with the averages obtained for 20 overnight EEG recordings analyzed in this study, as well as with the results reported previously in literature as inter-subject averages of solutions for spectral integrals, computed on visually selected spindles.

1 Introduction

In recent decades electroencephalography is losing field to the new brain imaging techniques like MRI/fMRI and PET. This is mainly due to the fact that these *imaging* techniques provide information directly related to the well known anatomy of the brain at a scale of few millimeters, which is more appealing and easier to interpret for the clinicians.

Nevertheless, EEG (together with MEG) still has the highest temporal resolution, and provides information directly related to the *function* of the brain—all from a relatively cheap and non-invasive technique. Therefore, several attempts were directed at relating the structures, known from the EEG traces, to the anatomical locations of their cerebral generators. Unfortunately, this so called EEG inverse problem is ill-posed and underdetermined (c.f. Koles (1998)). There is an infinity of possible electric current density distributions in the brain which may generate the same potential on the scalp surface. Choosing a unique solution requires a priori information, independently of the EEG data, which are usually an arbitrary choice of additional constraints.

There can be different kinds of constraints, the most used being of anatomical and physical-mathematical nature. The former consist basically on restricting the solution to some physiologically supported area, which can be a particular structure or the whole gray matter. The latter vary from considering the solution to be a sum of current dipoles to choosing the distributed solution with minimum norm or maximum smoothness. On the other hand, the task of solving an ill-posed problem by adding additional information about the solution has been firstly treated by the Tikhonov regularization (Pascual-Marqui et al., 1994; Wang et al., 1992; Hämäläinen and Ilmoniemi, 1994). Recently, the Bayesian approach has gained adepts because of its possibilities in introducing a priori information in a natural and flexible way (Schmidt et al., 1999; Trujillo-Barreto et al., 2004). Other approaches and combinations of the previously mentioned with time series and Fourier analysis have appeared in this field as well. According to constraints and algorithms used, different solutions are being promoted by different groups: LAURA, EPIFOCUS (Grave de Peralta-Menendez and Gonzales-Andino, 2002), ELECTRA (Grave de Peralta-Menendez et al., 2000)—and probably the most popular LORETA (Pascual-Marqui et al., 1994), with variants such as sLORETA (Pascual-Marqui, 2002), VARETA (Bosch-Bayard et al., 2001) and Bayesian

Email addresses: durka@fuw.edu.pl (Piotr J. Durka), amatys@fuw.edu.pl (Artur Matysiak), eduardo@cneuro.edu.cu (Eduardo Martínez Montes), peter@cneuro.edu.cu (Pedro Valdés Sosa), kjbli@fuw.edu.pl (Katarzyna J. Blinowska).

¹ supported by the grant of Committee for Scientific Research (Poland) to the Institute of Experimental Physics, Warsaw University.

Model Averaging solution (Trujillo-Barreto et al., 2004).

Just from the abundance of different solutions, one can see that the issue is complicated and far from stable conclusions, since none of the methods mentioned above gives fully satisfactory results in all kinds of EEG data. In this regard, an inverse solution is preferred according to the case of study. Some of them are suitable for applications in which a small region of the brain is active (as is the case for example in evoked potential studies) and others when the current density spread out in wider areas (e.g. spontaneous EEG, tumors, epilepsy). On the other hand, most of them, particularly Loreta, present usually physiologically non-interpretable sources, called ghost sources, and an inherent incapacity for recovering deep sources (Trujillo-Barreto et al., 2004). This bias on the recovering of the source amplitude is particular important when there exist more than one active source. The solution tends to present the cortical one (or nearer the electrodes) larger than the others, usually masking some strong activations in important deep structures of the brain. This is one of the motivations for the continuous developing of new methodologies for inverse solutions, although it has been shown that the bias can be overcome with a statistical postprocessing of the solution (Bosch-Bayard et al., 2001).

1.1 Motivation of this study

The scalp EEG is generally considered to be a linear sum of multiple neural masses or generators' electrical activity (Lopes Da Silva, 1999). Each of these generators, apart from its different localization, usually has a particular spectral content (probably with a signature very far from a delta function), and even a particular temporal evolution of its spectrum. This fact has brought neuroscientists to the task of decomposing the EEG into a sum of what can be called atoms of the electrical activity of the brain. Most of atomic decompositions of the EEG have taken into account two of the three inherent dimensions of this data, such as the space-time decompositions by Principal and Independent Component Analysis (PCA and ICA: Lagerlund et al. (1997); Cichocki and Amari (2002); Hyvarinen et al. (2001)), time-frequency analysis with the use of windowed Fourier transform (Makeig, 1993), wavelet transformation (Tallon-Baudry et al., 1997; Bertrand et al., 1994; Bartnik et al., 1992) and matching pursuit algorithm (Durka and Blinowska, 1995). Recently, new attempts of finding a multidimensional (space-time-frequency) atomic decomposition of the EEG have been made, in the way of having a complete description of the electrical activity of the underlying neural masses (König et al., 2001; Miwakeichi et al., 2004; Martínez-Montes et al., 2004).

On the other hand, inverse solutions have been mostly applied to instantaneous data (i.e. time points of the EEG data are treated separately), although

some advances have been made to incorporate the temporal information for obtaining more reliable solutions (Yamashita et al., 2004; Galka et al., 2004). In the frequency domain, inverse solutions can be used as well due to the linearity of Fourier transform. However, in this case, clear delineation of the sources of activity usually requires heavy statistical post-processing of repetitions or many subjects data. This is probably due to the fact that the model underlying the inverse solution relates directly to energies of one or few generators, measured at the scalp. Unfortunately, spectral integrals used as the input to these procedures incorporate also large amount of unrelated activity. For example, in (Anderer et al., 2001) spectral analysis was performed on 1.25 sec time epochs with 0.8 Hz resolution in frequency; the content of these $1.25 \text{ s} \times 0.8 \text{ Hz}$ boxes, which is due to the activity of sleep spindles generators, may at best statistically dominate other contributions. This effect, illustrated in Figure 1, is a direct consequence of the uncertainty principle in signal analysis (Mallat, 1999).

[Fig. 1 about here.]

In this study we will present a new approach for source localization of single structures with definite spatial-time-frequency properties. As a first step, EEG recordings are decomposed into a sum of atoms, each being the product of spatial (topographic) signature and waveforms having determined time-frequency localization. This is achieved by the multichannel matching pursuit algorithm, which is a generalization of the matching pursuit to analyzing several signals simultaneously, i.e. multidimensional data. The second step consist of using the topographic signatures of atoms of interest as input for obtaining 3D localization of its cerebral sources. This can be done through the use of any of the known inverse solutions methods. In searching of simplicity and clear understanding of the method, we will use the widely known Low Resolution Electromagnetic Tomography (LORETA). It will be shown that application of selective and high-resolution estimates of generators activity, symbolically presented in Figure 1b and described in Section 2.1, significantly improves the robustness of EEG inverse solutions. As will be presented in the following sections, it allows for a repeatable localization of single structures, based upon their time-frequency signatures.

2 Methods

2.1 Multichannel matching pursuit (MMP)

Matching pursuit algorithm (MP) with time-frequency dictionaries was proposed by Mallat and Zhang (1993) as a suboptimal iterative solution to the

problem of optimal representation of monochannel signal in a redundant dictionary. Bias-free version, proposed by Durka et al. (2001), relies on randomization of the parameters of Gabor functions forming the dictionary. Real valued Gabor function can be expressed as

$$\mathbf{g}_\gamma(t) = K(\gamma)e^{-\pi\left(\frac{t-u}{s}\right)^2} \cos(\omega(t-u) + \phi), \quad (1)$$

where $\gamma = \{u, \omega, s, \phi\}$ and $K(\gamma)$ is such that $\|\mathbf{g}_\gamma\| = 1$. Dictionary contains also Dirac and Fourier bases. From this dictionary, in each step we chose the atom representing optimally the n -th residuum $R^n f$ of the signal f , left from previous iterations. For a monochannel signal f it can be written as

$$\begin{cases} R^0 f = f \\ R^n f = \langle R^n f, g_{\gamma_n} \rangle g_{\gamma_n} + R^{n+1} f \\ g_{\gamma_n} = \arg \max_{g_{\gamma_i} \in D} |\langle R^n f, g_{\gamma_i} \rangle| \end{cases} \quad (2)$$

This greedy algorithm can fail to properly decompose certain signals, containing simple combination of dictionary’s functions. Theoretical examples of such failures are given e.g. by DeVore and Temlyakov (1996); Chen et al. (2001); Durka (2003). However, this suboptimality does not seem to pose problems in the parameterization of the EEG time series, as proved by 10 years of successful applications.² Recently it was shown that such “failures” may be explored to distinguish rhythmic discharges from series of unrelated/desynchronized spikes (Durka, 2004).

Multichannel extension of the MP algorithm (MMP) can be achieved in many ways. It is imaginable e.g. to allow for slightly different phases of the Gabor atoms (1) in different channels—phase optimization is usually a separate step in the numerical implementations. Differences in these phases might possibly reveal the direction of the information flow between channels, as in the AR-based Directed Transfer Function (Kamiński and Blinowska, 1991)—in this case this flow would be attributed to a specified, single structure.³ Since in this study the MMP was intended as preprocessing for instantaneous EEG inverse solutions, we keep the phases constant across the channels, assuming each atom corresponds to the same activity in all of them, as discussed in the next section.

² For a review see e.g. (Durka and Blinowska, 2001; Durka, 2003) plus a recent work on ERD/ERS (Durka et al., 2004)

³ However it is not obvious whether the information, contained in the EEG time series collected with the standard resolution, would suffice to estimate such a magnitude from single epochs.

Criterion for selecting the atom which “best” fits the residuum in all channels \mathbf{f}^i of the multichannel signal \mathbf{f} can be taken as

$$\max_{g_{\gamma_n} \in D} \sum_i |\langle R^n \mathbf{f}^i, g_{\gamma_n} \rangle|^2 \quad (3)$$

(Gribonval, 2003). This choice relates to the maximum of the energy of the multichannel signal, explained in one iteration. However, we may also choose e.g.

$$\max_{g_{\gamma_n} \in D} \sum_i |\langle R^n \mathbf{f}^i, g_{\gamma_n} \rangle|. \quad (4)$$

Algorithms based upon (3) and (4) may differ in convergence, but a structure from the dictionary, clearly present in \mathbf{f} , should be parameterized equally by both implementations, possibly in a different iteration. Slight differences in estimated parameters may stem from the nonlinearity of the algorithm.

In this study we choose the MMP maximizing the plain sum of products: $\max_{g_{\gamma_i} \in D} |\sum_i \langle R^n \mathbf{f}^i, g_{\gamma_i} \rangle|$. Owing to the linearity of the residuum operator R (properties 1–2 presented in the Appendix), this choice allows for an efficient implementation. Instead of finding in each step the product of each dictionary’s waveform with all the channels, and then finding the maximum of the sum of these products (as in Eq. 4) or their squares (as in Eq. 3), in each step we decompose the signal constructed as the sum of all the channels residua, and then find the product of the globally optimal waveform with each channel. Denoting the average of all the N_e channels as $\bar{\mathbf{f}} = \frac{1}{N_e} \sum_{i=1}^{N_e} \mathbf{f}^i$, we define the algorithm as:

$$\begin{cases} R^0 \bar{\mathbf{f}} = \bar{\mathbf{f}} \\ R^n \bar{\mathbf{f}} = \langle R^n \bar{\mathbf{f}}, \mathbf{g}_{\gamma_n} \rangle \mathbf{g}_{\gamma_n} + R^{n+1} \bar{\mathbf{f}} \\ \mathbf{g}_{\gamma_n} = \arg \max_{\mathbf{g}_{\gamma} \in D} |\langle R^n \bar{\mathbf{f}}, \mathbf{g}_{\gamma} \rangle| \\ R^n \mathbf{f}^i = \langle R^n \mathbf{f}^i, \mathbf{g}_{\gamma_n} \rangle \mathbf{g}_{\gamma_n} + R^{n+1} \mathbf{f}^i \end{cases} \quad (5)$$

This decomposition conserves the energy of representation (property 3 in the Appendix); however, its convergence may be severely impaired in special cases, when given waveform is present in different channels with exactly opposite phases, with weights causing its total cancellation in the average signals $R^n \bar{\mathbf{f}}$. Nevertheless, if this cancellation is not *complete*, and a clear trace of the atom g_{γ_n} is still present in $R^n \bar{\mathbf{f}}$, then it should be correctly parameterized by the products $\langle R^n \mathbf{f}^i, \mathbf{g}_{\gamma} \rangle$ —probably in a later iteration as compared to the algorithm maximizing the sum of moduli or squares, since $\sum |\langle R^n \mathbf{f}^i, g_{\gamma_n} \rangle| \geq |\sum \langle R^n \mathbf{f}^i, g_{\gamma_n} \rangle|$. As mentioned above, additional differences in $\langle R^n \mathbf{f}^i, g_{\gamma_n} \rangle$ for

different n may also stem from the nonlinearity of the MP algorithm, but in general, except for a very special cases of total cancellation of a structure in the average of all channels, γ_n and $\langle R^n \mathbf{f}^i, g_{\gamma_n} \rangle$ obtained from this approach should be equivalent to those returned by an algorithm maximizing (3) or (4). We may say that this flavor of MMP favours structures with equal phases in all the channels.⁴

As a reward, this procedure reduces the computational complexity by the factor N_e (that is number of channels). In this study $N_e = 21$, but in general for inverse solutions a larger number of derivations (e.g. 128) is suitable. Speed of computations is still an important factor in practical applications, since the unbiased implementations of MP (Durka et al., 2001) make it difficult to apply some most natural numerical optimizations (this work is still in progress), and unbiased MP is still computationally intensive.

Due to operating on the average of channels, this version of the algorithm cannot be directly applied to the data presented in the average reference. In this study, we performed the MMP computations on the original EEG signals, which are referenced to the linked ears (A1+A2). The output of this procedure are the time-frequency atoms representing the structures of interest, and the corresponding coefficients for each electrode given by the products $\langle R^n \mathbf{f}^i, g_{\gamma_n} \rangle$. This vector represents a topographic (spatial) signature (see examples in lower panel of figure 2) of the n -th atom, and completes the picture of a space-time-frequency decomposition of the EEG data. As will be explained in the next section, these topographic signatures conserve the magnitude of the original data (since the gabor atoms are normalized) and the reference to linked ears. Then these topographic signatures are taken as the input for a source localization procedure.

2.2 Inverse solution

Three dimensional reconstruction of the current densities inside the brain, obtained from the inverse solutions, is commonly termed brain electrical tomography (BET). The term “tomography” is also explicitly present in the acronym of the method used in this study: LORETA stands for “LOW Resolution Electromagnetic TomogrAphy”. However, due to the problems mentioned in the Introduction, it may lead to serious misunderstandings when e.g. directly comparing the clinical applicability of BET and CT. Therefore, in the following we will avoid the use of the term “tomography”, and will use “inverse solution” or “source estimation/localization” indistinctly.

⁴ This feature will be more relevant e.g. for compression, where the index of the iteration n may be used as a cutoff criterion.

The relation between scalp surface EEG measurements and the primary current density is described by a linear equation:

$$\mathbf{a} = \mathbf{K}\mathbf{j} + \mathbf{e} \quad (6)$$

Here, \mathbf{a} denotes the vector containing the scalp electric potentials at N_e electrodes. The vector \mathbf{j} has thrice the number of voxels elements, corresponding to the x , y and z components of the primary current density vector in each voxel of a grid defined inside the brain. The matrix \mathbf{K} , linking the current density with the measurements, is called the lead field matrix. It can be calculated by applying Maxwell's equations to a particular head model (Nunez, 1981). The vector \mathbf{e} is an additive random element representing unmodeled effects such as observation noise. In the case of the data being a matrix \mathbf{A} with N columns (representing e.g. time points, trials, atoms), this formulation will be the same with corresponding N columns in a matrix \mathbf{J} .

The inverse problem is defined as the estimation of current density \mathbf{j} from a given measurement \mathbf{a} and constitutes an ill-conditioned (sensitive to noise) and ill-posed problem in the sense of Hadamard (Hadamard, 1923), since it has non-unique solution. This is easy to see from the fact that the number of scalp electrodes is much smaller than the number of voxels for which the current density has to be estimated. Therefore, the imposition of additional constraints on the solution is needed to obtain a unique solution. This can be done by several approaches such as the Regularization Theory of Tikhonov like Loreta (Pascual-Marqui et al., 1994) and Bayesian Theory (Trujillo-Barreto et al., 2004) and/or using anatomical and other physical constraints like assuming the current density to consist only of single current dipoles (De Munck, 1989; Scherg and von Cramon, 1986; Scholz and Schwierz, 1994).

Another aspect to take into account is the ambiguity of voltage differences with respect to the reference. Although this is not a problem for the inverse solution procedure if the lead field is computed with the same reference used for recording the data, it has been shown (Pascual-Marqui, 1995) that Loreta solution is valid for equation (6) when the scalp voltage differences as well as the lead field are taken to have average reference. This relates to the fact that some practical or technical solutions for the reference in measuring the EEG, such as the linked ears, does not represent a physical reference, i.e it can not be located in a particular position in space. That is why the use of average reference is a common practice as preprocessing of the data for solving the EEG inverse problem and it is easily achieved by pre multiplication of both the data and the lead field by the matrix $\mathbf{H} = \mathbf{I} - \mathbf{1}\mathbf{1}^T/N_e$. Here \mathbf{I} is the identity matrix of size N_e , $\mathbf{1}$ is a N_e -vector of ones, and $\mathbf{1}^T$ denotes its transpose.

In this study we used the implementation of an inverse solution (hereinafter Loreta solution), developed in the Cuban Neuroscience Center, which uses

three concentric spheres model with solution space constrained to cortical gray matter and hippocampus (based upon the human brain atlas by Talairach and Tournoux (1988)). The lead field was computed as defined by Riera and Fuentes (1997), and Loreta algorithm (Pascual-Marqui et al., 1994) was used with an automatic setting of regularization parameter based on the minimization of the generalized cross-validation function. The average Probabilistic MRI Atlas produced by the Montreal Neurological Institute (Collins et al., 1994; Evans et al., 1993, 1994; Mazziotta et al., 1995) was used for computation and representation of Loreta inverse solutions.

This methodology was applied for source localization of single atoms with specific time-frequency characteristics, found from adaptive decomposition of EEG time series by MMP (Section 2.1). In a matrix notation, MMP representation of a spatio-temporal EEG recording \mathbf{F} ⁵ in N_a atoms is expressed as the product of two matrices plus the $N_a + 1$ residual:

$$\mathbf{F}_{N_e \times N_t} = \mathbf{A}_{N_e \times N_a} \mathbf{G}_{N_a \times N_t} + R^{N_a+1} \mathbf{F}_{N_e \times N_t} \quad (7)$$

The rows of matrix \mathbf{G} are the \mathbf{g}_{γ_n} ($n = 1 \dots N_a$) fitted by MMP to the signal \mathbf{F} . The i -th element of n -th column of matrix \mathbf{A} is the scalar product $\langle R^n \mathbf{f}^i, \mathbf{g}_{\gamma_n} \rangle$.

The square of these elements gives the energy explained by the n -th atom fitted in the i -th channel, since dictionary functions \mathbf{g}_{γ_n} are normalized. From the linearity of the procedure (see Appendix) it is easy to see that these signatures will have the same reference as the original EEG data. In this study, the data is referenced to the linked ears and therefore, so will be the topographic signatures. Values of these topographies can be positive or negative.

In the second (separate) step of the proposed method, the spatial 3D localization of the sources of single atoms is carried out from each topography according to Equation 6. For this purpose, the topographic signatures are taken to have average reference as required by LORETA (Pascual-Marqui, 1995), but this does not imply any further assumption or transformation on the data than those already made in the first step (MMP decomposition).

2.3 Parameterization of sleep spindles

In the last decade matching pursuit with Gabor dictionary was successfully applied in monochannel analysis of several types of EEG signals—for review see e.g. (Durka and Blinowska, 2001; Durka, 2003). Reliability of detection

⁵ In the other sections and equations, multichannel signal forming the matrix \mathbf{F} is denoted by \mathbf{f} , and the one-dimensional signal in channel i as \mathbf{f}^i ($i = 1 \dots N_e$)

and parameterization of sleep spindles in single EEG channels was presented by Żygierewicz et al. (1999) and Durka et al. (2002). In this study, structures corresponding to sleep spindles were automatically chosen from the matching pursuit decompositions of artifact-free epochs of stage 2, as Gabor functions with frequency from 11.5 to 14.5 Hz and width from 0.5 to 2 seconds. Minimum peak-to-peak amplitude of a structure classified as sleep spindle was determined separately for each recording, to take into account inter-subject differences in EEG amplitude, depending e.g. on age, sex (Danker-Hopfe et al., 2004; Larsen et al., 1995) and quality of sleep (Armitage et al., 2000). Due to the one-to-one relation between the sleep spindles and fitted Gabor atoms (c.f. Żygierewicz et al. (1999) and Figure 2), this procedure provides an automatic parameterization of all the sleep spindles, present in given recording, in terms of their: time positions, lengths, frequencies and amplitudes in each channel (that is topographies, as discussed in section 2.1).

[Fig. 2 about here.]

2.4 *Experimental Data*

We analyzed 20 overnight polysomnographic recordings, recorded at Medical University of Warsaw, Chair of Psychiatry, as a control group of another study. Polygraphic monitoring consisted of EEG activity collected from 21 electrodes, according to the international 10–20 system, electrooculogram (EOG) from two channels, and submentalis electromyogram. Filters were set between 0.15 and 30.0 Hz. The impedance at each electrode was below 5000 ohms. Sleep stages and artifacts were identified visually (stages according to the standardized manual for sleep scoring (Rechtschaffen and Kales, 1968)). Informed consent was obtained from all subjects. The study was approved by the University Ethics Committee.

3 Results

Sleep spindles were automatically detected in artifact-free epochs of stage 2. Each of the 20 available multichannel overnight EEG recordings (Section 2.4) was decomposed by the MMP algorithm described in section 2.1. Atoms corresponding to sleep spindles were selected from this decomposition according to the parameters described in section 2.3, and intensity images were obtained for each of these structures separately by means of the procedure described in section 2.2. Figure 3 presents Loreta images obtained for single sleep spindles: in each of the frequency bands, covering the spindles band in 0.5 Hz steps, one sleep spindle was randomly chosen from one of the analyzed recordings.

[Fig. 3 about here.]

Based upon preliminary inspection of Loreta images as in Figure 3, as well as their averages per subject, we divided the available recordings in two groups:

- (1) In five of these subjects, Loreta images showed higher values for slower spindles consistently concentrated in the anterior regions.
- (2) In the remaining 15 subjects, topographical distinction between the fast and slow spindles was not so clear.

The average number of spindles detected per one overnight recording in the first group was 578 (std. dev. 120), in the second group—692 (std. dev. 316). Figures 4 and 5 present averages of single Loreta images—like the one presented in Figure 3—separately for the subjects from these two groups. These images are constructed as vertical slices of the raw Loreta solution for the given structure, without any statistical postprocessing of the results. We observe the general consistency of these average images with the images obtained for single sleep spindles (Figure 3), as well as their concordance with previous results, in particular those presented by (Anderer et al., 2001). In that study, construction of average images (corresponding to Figures 4 and 5) from inverse solutions applied to spectral integrals required additional steps:

- visual selection of sleep spindles,
- their assignment to different classes of topographic distribution (also visual),
- subtracting from the obtained images corresponding distributions, computed for the visually selected non-spindle EEG epochs.

In this paper, we automatically included all the spindles conforming to the general criteria—several hundreds per subject, comparing to an order of magnitude less of the structures, carefully selected by Anderer et al. (2001). As a result, images presented in that study look slightly sharper than Figures 4 and 5.

[Fig. 4 about here.]

[Fig. 5 about here.]

4 Discussion

This paper implements a complete algorithm, starting from the raw EEG data and classical definition of sleep spindles, giving as the output automatic detection and description of structures conforming to these criteria. Each of the detected spindles is localised in time, frequency and space. Advantages of this paradigm include spatial localisation of single sleep spindles, straightforward

extension to other kinds of structures, high degree of compatibility with the visual EEG analysis and a relative freedom from arbitrary parameters.

However, the idea of using topographic signatures of time-frequency atoms as the input for inverse solutions is not entirely new. Matching pursuit with a limited dictionary of wavelets was used for analysis of evoked potentials by Geva (1998), and localization of the sources of these atoms was carried out by a linear exhaustive search. Sources were constrained to a particular grid of the brain and supposed to be single or symmetrical pair of current dipoles. In a different study, another kind of inverse solution, called Source Spectra Imaging (SSI), was used for finding the spectra of the current density distribution, after obtaining topographic signatures from three-dimensional decomposition of the spontaneous EEG time-varying spectrum (Miwakeichi et al., 2004; Martínez-Montes et al., 2004). On the other side, multichannel extension of the MP was previously discussed by Gribonval (2003). It was applied to the separation of sources from stereo signals (Gribonval, 2002).

A different preprocessing for the inverse solutions can be based upon Independent Component Analysis (Tang et al., 2002). Contrary to the atoms identified within the proposed approach, independent components are not a priori related to any structures known from the clinical analysis of EEG. Also, ICA is based upon several strong assumptions, e.g. linearity and stability of the mixing process and some statistical independence of the sources.

In this study we combine adaptive time-frequency parameterization of EEG structures and EEG source localization. Resulting solution is not restricted to a sum of single current dipoles as in (Geva, 1998), and avoids strong assumptions on the independence of generators activity, made by the SSI solution (Miwakeichi et al., 2004). Sub-optimal implementation of the multichannel matching pursuit, based upon decomposition of the average residuum in each iteration, allows for a significant gain in the speed of computations. It seems that its suboptimality does not deteriorate the detection of relevant EEG structures; however, possible advantages of the other discussed implementations remain to be tested in this context.

Results obtained hereby on 20 overnight EEG recordings are coherent with the general knowledge about sleep spindles, and with particular results obtained by Anderer et al. (2001) with critical involvement of the visual analysis. As a new element, illustrating the increase of sensitivity compared to the previous approaches, we obtain possibility of localizing single structures. These results were obtained by a plain, raw and automatic combination of MMP and Loreta, with an explicit implementation of the traditional definition of sleep spindles. It was intended only as presentation of the possibilities and basic experimental verification. A wide margin for improvements remains open for applications, addressing directly some physiological or clinical issues: starting from the care-

ful selection of the EEG epochs and tuning the parameters defining relevant structures (in this study sleep spindles), to the final statistical post-processing.

Some issues, like e.g. correction for the localization bias of the Loreta solution, remain to be solved within the proposed framework. It will be also valuable to test MMP as preprocessing to other inverse EEG solutions.

Reproducible research

An implementation of the MMP algorithm, described in Section 2.1 (with complete source in C), is available from <http://eeg.pl>, section “Software”. Matlab code for the Loreta inverse solution is available upon request from Eduardo Martínez Montes (eduardo@cneuro.edu.cu).

Acknowledgments

We thank Prof. Waldemar Szelenberger from the Warsaw Medical School for providing the EEG data, Marek Barwiński for efficient implementation of the fast matching pursuit algorithm, and Dr. Jorge Bosch-Bayard for offering his technical experience on the inverse solution procedure.

Appendix: Properties of the proposed implementation of multichannel matching pursuit

Property 1 (Linearity) *The sum of residua is equal to residuum of the sum, which implies that R^n is a linear operator.*

$$R^n \bar{\mathbf{f}} = R^n \frac{1}{N_e} \sum_{i=1}^{N_e} \mathbf{f}^i = \frac{1}{N_e} \sum_{i=1}^{N_e} R^n \mathbf{f}^i = \overline{R^n \mathbf{f}} \quad (8)$$

Proof: From the fact that operator R^0 is an identity operator (i.e. $R^0 \mathbf{f} = \mathbf{f}$) we have:

$$R^0 \sum_{i=1}^{N_e} \mathbf{f}^i = \sum_{i=1}^{N_e} R^0 \mathbf{f}^i \quad (9)$$

The linearity of product operator $\langle *, * \rangle$ implies

$$\left\langle \frac{1}{N_e} \sum_{i=1}^{N_e} R^n \mathbf{f}^i, \mathbf{g}_{\gamma_n} \right\rangle = \frac{1}{N_e} \sum_{i=1}^{N_e} \langle R^n \mathbf{f}^i, \mathbf{g}_{\gamma_n} \rangle \quad (10)$$

From the above, for the 0-th iteration the residuum operator R^0 is a linear operator.

$$\frac{1}{N_e} \sum_{i=1}^{N_e} (R^0 \mathbf{f}^i - \langle R^0 \mathbf{f}^i, \mathbf{g}_{\gamma_0} \rangle \mathbf{g}_{\gamma_0}) = \frac{1}{N_e} \sum_{i=1}^{N_e} R^1 \mathbf{f}^i = R^1 \frac{1}{N_e} \sum_{i=1}^{N_e} \mathbf{f}^i \quad (11)$$

By induction for $n > 0$ -th iteration we have:

$$\frac{1}{N_e} \sum_{i=1}^{N_e} (R^n \mathbf{f}^i - \langle R^n \mathbf{f}^i, \mathbf{g}_{\gamma_n} \rangle \mathbf{g}_{\gamma_n}) = \frac{1}{N_e} \sum_{i=1}^{N_e} R^{n+1} \mathbf{f}^i = R^{n+1} \frac{1}{N_e} \sum_{i=1}^{N_e} \mathbf{f}^i \quad (12)$$

Property 2 *The sum of products across all channels is equal to product of the sum*

$$\langle R^n \bar{\mathbf{f}}, \mathbf{g}_{\gamma_n} \rangle = \frac{1}{N_e} \sum_{i=1}^{N_e} \langle R^n \mathbf{f}^i, \mathbf{g}_{\gamma_n} \rangle \quad (13)$$

Proof: It is a simple conclusion from linearity of the residuum operator R^n .

Property 3 (Energy conservation) *The energy of the decomposed signal is conserved across all channels*

$$\|\bar{\mathbf{f}}\|^2 = \sum_{n=0}^{N_a} \left| \frac{1}{N_e} \sum_{i=1}^{N_e} \langle R^n \mathbf{f}^i, \mathbf{g}_{\gamma_n} \rangle \right|^2 + \left\| \frac{1}{N_e} \sum_{i=1}^{N_e} R^{N_a+1} \mathbf{f}^i \right\|^2 \quad (14)$$

$$\|\mathbf{f}^i\|^2 = \sum_{n=0}^{N_a} |\langle R^n \mathbf{f}^i, \mathbf{g}_{\gamma_n} \rangle|^2 + \|R^{N_a+1} \mathbf{f}^i\|^2 \quad (15)$$

Proof: The orthogonality of $R^{n+1} \bar{\mathbf{f}}$ or $R^{n+1} \mathbf{f}^i$ with \mathbf{g}_{γ_n} implies energy conservation for the average signal $\bar{\mathbf{f}}$ and its every channel \mathbf{f}^i .

References

Anderer P, Klösch G, Gruber G, Trenker E, Pascual-Marqui R, Zeitlhofer J, Barbanoj M, Rappelsberger P, Saletu B. Low-resolution brain electromagnetic tomography revealed simultaneously active frontal and parietal sleep spindles sources in the human cortex. *Neuroscience*, 2001; 103 (3): 581–592.

- Armitage R, Hoffmann R, Fitch T, Trivedi M, Rush A. Temporal characteristics of delta activity during nrem sleep in depressed outpatients and healthy adults: group and sex effects. *Sleep*, 2000; 23 (5): 607–617.
- Bartnik EA, Blinowska KJ, Durka PJ. Single evoked potential reconstruction by means of wavelet transform. *Biol Cybern*, 1992; 67: 175–181.
- Bertrand O, Bohorquez J, Pernier J. Time-frequency digital filtering based on an invertible wavelet transform: an application to evoked potential. *IEEE Trans Biomed Eng*, 1994; 41: 77–88.
- Bosch-Bayard J, Valdes-Sosa P, Virues-Alba T, Aubert-Vazquez E, John ER, Harmony T, Riera-Diaz J, Trujillo-Barreto N. 3D statistical parametric mapping of EEG source spectra by means of variable resolution electromagnetic tomography (VARETA). *Clinical Electroencephalography*, 2001; 32.
- Chen SS, Donoho DL, Saunders MA. Atomic decomposition by basis pursuit. *SIAM Review*, 2001; 43 (1): 129–159.
- Cichocki A, Amari S. *Adaptive Blind Signal and Image Processing*. John Wiley & Sons, Ltd., 2002.
- Collins D, Neelin P, Peters R, Evans A. Automatic 3D intersubject registration of mr volumetric in standardized Talairach space. *J Comput Assist Tomogr*, 1994; 18: 192–205.
- Danker-Hopfe H, Kunz D, Gruber G, Klosch G, Lorenzo J, Himanen S, Kemp B, Penzel T, Roschke J, Dorn H, Schlogl A, Trenker E, Dorffner G. Interrater reliability between scorers from eight european sleep laboratories in subjects with different sleep disorders. *Journal of Sleep Research*, 2004; 13 (1): 63–9.
- De Munck J. Random dipoles as a model for spontaneous eeg and meg activity. In: S.J. Williamson, editor. *Advances in Biomagnetism*. New York, 1989: 595–598.
- DeVore RA, Temlyakov VN. Some remarks on greedy algorithms. *Advances in Computational Mathematics*, 1996; 5: 173–187.
- Durka PJ. From wavelets to adaptive approximations: time-frequency parametrization of EEG. *BioMedical Engineering OnLine* 2 (1).
- Durka PJ. Adaptive time-frequency parametrization of epileptic EEG spikes. *Physical Review E*, 2004; 69: (051914).
- Durka PJ, Szelenberger W, Blinowska K, Androsiuk W, Myszka M. Adaptive time-frequency parametrization in pharmaco EEG. *Journal of Neuroscience Methods*, 2002; 117: 65–71.
- Durka PJ, Żygierewicz J, Klekowicz H, Ginter J, Blinowska K. On the statistical significance of event-related EEG desynchronization and synchronization in the time-frequency plane. *IEEE Transactions on Biomedical Engineering*, 2004; 51: 1167–1175.
- Durka PJ, Blinowska KJ. Analysis of EEG transients by means of matching pursuit. *Ann Biomed Eng*, 1995; 23: 608–611.
- Durka PJ, Blinowska KJ.. A unified time-frequency parametrization of EEG. *IEEE Engineering in Medicine and Biology Magazine*, Sept/Oct 2001; 20 (5): 47–53.

- Durka PJ, Ircha D, Blinowska KJ. Stochastic time-frequency dictionaries for matching pursuit. *IEEE Tran Signal Process*, March 2001; 49 (3): 507–510.
- Evans A, Collins D, Mills S, Brown E, Kelly R, Peters T. 3D statistical neuroanatomical models from 305 MRI volumes. In: *Proc. IEEE-Nuclear Science Symposium and Medical Imaging Conference*, M.T.P Press, London, 1993; 95: 1813–1817.
- Evans A, Collins D, Neelin P, MacDonald D, Kamber M, Marrett T. Three-dimensional correlative imaging: applications in human brain mapping. In: Thatcher, R., Hallet, M., Zeffiro, T., John, E., Huerta, M. (Eds.), *Functional Neuroimaging: Technical Foundations*. Academic Press, New York, 1994: 145–161.
- Galka A, Yamashita O, Ozaki T, Biscay R, Valdés-Sosa P. A solution to the dynamical inverse problem of EEG generation using spatiotemporal kalman filtering. *NeuroImage*, 2004; 23: 435–453.
- Geva A. Bioelectric sources estimation using spatio-temporal matching pursuit. *Applied Signal Processing*, 1998; 5: 195–208.
- Grave de Peralta-Menendez R, Gonzales-Andino S. Comparisons of algorithms for the localization of focal sources: evaluation with simulated data and analysis of experimental data. *IJBEM*, 2002; 4 (1).
- Grave de Peralta-Menendez R, Gonzales-Andino S, Morand S, Michel C, Landis T. Imaging the electrical activity of the brain: ELECTRA. *Human Brain Mapping*, 2000; 9: 1–12.
- Gribonval R. Sparse decomposition of stereo signals with matching pursuit and application to blind separation of more than two sources from a stereo mixture. In: *Proc. Int. Conf. Acoust. Speech Signal Process. (ICASSP 02)*. Orlando, Florida, May 2002.
- Gribonval R. Piecewise linear source separation. In: *Proc. SPIE 03. Vol. 5207 Wavelets: Applications in Signal and Image Processing*. Sang Diego, California, August 2003.
- Hadamard J. *Lecture on the Cauchy problem in linear partial differential equations*. Yale University Press, New Haven, CT, 1923.
- Hämäläinen M, Ilmoniemi R. Interpreting magnetic fields of the brain: minimum norm estimates. *Med Biol Eng Comput*, 1994; 32: 35–42.
- Hyvarinen A, Karhunen J, Oja E. *Independent Component Analysis*. John Wiley & Sons, Inc., 2001.
- Kamiński M, Blinowska K. A new method of the description of the information flow. *Biological Cybernetics*, 1991; 65: 203–210.
- Koles Z. Trends in EEG source localization. *Electroenceph Clin Neurophysiol*, 1998; 106: 127–137.
- König T, Marti-Lopez F, Valdes-Sosa P. Topographic time-frequency decomposition of the EEG. *NeuroImage*, 2001; 14: 383–390.
- Lagerlund T, Sharbrough F, Busacker N. Spatial filtering of multichannel electroencephalographic recordings through principal component analysis by singular value decomposition. *J Clin Neurophysiol*, 1997; 14: 73–83.
- Larsen L, Moe K, Vitiello M, Prinz P. A note on the night-to-night stability of

- stages 3+4 sleep in healthy older adults: a comparison of visual and spectral evaluations of stages 3+4 sleep. *Sleep*, 1995; 18: 7–10.
- Lopes Da Silva F. EEG analysis: Theory and practice. In: *Electroencephalography: Basic Principles, Clinical Applications and Related Fields*, 4th Edition. Williams & Wilkins, 1999: 1135–1163.
- Makeig S. Auditory event-related dynamics of the EEG spectrum and effects of exposure to tones. *Electroencephalogr Clin Neurophysiol*, 1993; 86: 283–293.
- Mallat, S. *A wavelet tour of signal processing*, 2nd Edition. Academic Press, New York, 1999.
- Mallat S, Zhang Z. Matching pursuit with time-frequency dictionaries. *IEEE Transactions on Signal Processing*, Dec 1993; 41: 3397–3415.
- Martínez-Montes E, Valdés-Sosa P, Miwakeichi F, Goldman R, Cohen M. Concurrent EEG/fMRI analysis by multi-way partial least squares. *NeuroImage*, 2004; 22 (3): 1023–1034.
- Mazziotta J, Toga A, Evans A, Fox P, Lancaster J. A probabilistic atlas of the human brain: theory and rationale for its development. *NeuroImage*, 1995; 2: 89–101.
- Miwakeichi F, Martínez-Montes E, Valdés-Sosa P, Nishiyama N, Hiroaki M, Yamaguchi Y. Decomposing EEG data into space-time-frequency components using parallel factor analysis. *NeuroImage*, 2004; 22 (3): 1035–1045.
- Nunez P. *Electric Fields of the Brain*. Oxford University Press, 1981.
- Pascual-Marqui R. Reply to comments by hämäläinen, ilmoniemi and nunez. en source localization: Discussion of the inverse problem (W. Skrandies, ed.). *ISBET Newsletter*, 1995; (6): 16–28.
- Pascual-Marqui R. Standardized low-resolution brain electromagnetic tomography (sloreta): technical details. *Methods & Findings in Experimental & Clinical Pharmacology*, 2002; 24: 5–12.
- Pascual-Marqui R, Michel C, Lehman D. Low resolution electromagnetic tomography: a new method to localize electrical activity in the brain. *Int J Psychophysiol*, 1994; 18: 49–65.
- Rechtschaffen A, Kales A (Eds.). *A manual of standardized terminology, techniques and scoring system for sleep stages in human subjects*. No. 204 in National Institutes of Health Publications. US Government Printing Office, Washington DC, 1968.
- Riera J, Fuentes M. Electric lead field for a piece-wise homogeneous volume conductor model of the head. *IEEE Trans. on Biomed. Eng.*, 1998; 45: 746–753.
- Scherg M, von Cramon D. Evoked dipole source potentials of the human auditory cortex. *Electroencephalogr Clin Neurophysiol*, 1986; 65: 344–360.
- Schmidt D, George J, Wood C. Bayesian inference applied to the biomagnetic inverse problem. *Hum Brain Mapp*, 1999; 7: 195–212.
- Scholz B, Schwierz G. Probability-based current dipole localization from biomagnetic fields. *IEEE Trans Biomed Eng*, 1994; 41: 735–742.
- Talairach J, Tournoux P. *Co-Planar Stereotaxic Atlas of the Human Brain*.

- Stuttgart, 1988.
- Tallon-Baudry C, Bertrand O, Delpuech C, Pernier J. Oscillatory g-band (30–70 Hz) activity induced by a visual search task in humans. *J Neurosci*, 1997; 17: 722–734.
- Tang AC, Pearlmutter BA, Malaszenko NA, Phung DB, Reeb BC. Independent components of magnetoencephalography: Localization. *Neural Computation*, 2002; 14: 1827–1858.
- Trujillo-Barreto NJ, Aubert E, Valdés-Sosa P. Bayesian model averaging in EEG/MEG imaging. *NeuroImage*, 2004; 21: 1300–1319.
- Wang J, Williamson S, Kaufman L. Magnetic source images determined by a leadfield analysis—the unique minimum-norm least squares estimation. *IEEE T Bio-Med Eng*, 1992; 39: 231–251.
- Yamashita O, Galka A, Ozaki T, Biscay R, Valdés-Sosa P. Recursive penalized least squares solution for dynamical inverse problems of EEG generation. *Human Brain Mapping*, 2004; 21: 221–235.
- Żygierewicz J, Blinowska KJ, Durka PJ, Szelenberger W, Niemcewicz S, Androsiuk W. High resolution study of sleep spindles. *Clin Neurophysiol*, 1999; 110 (12): 2136–2147.

Figures

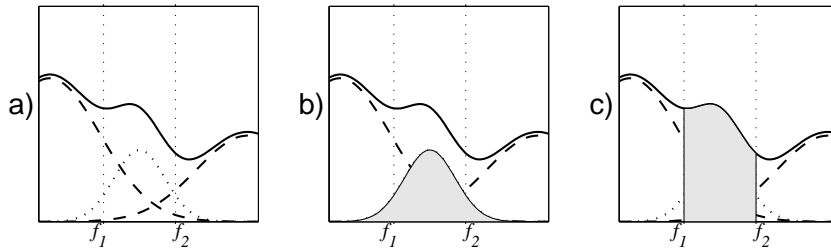


Fig. 1. Spectral power (vertical) versus frequency (horizontal) of three hypothetical structures with frequency centers lying inside (dotted) and outside (dashed line) the f_1 - f_2 interval. Due to the uncertainty principle, their spectral contents overlap. Solid line presents their sum, i.e. total spectral power, as estimated e.g. by Fourier transform. In b) we mark (shaded) the actual power carried by structure of frequency originating between f_1 and f_2 , as estimated e.g. by adaptive time-frequency approximation. Plot c) highlights the power obtained from a spectral integral from f_1 to f_2 . We observe that neighboring structures from outside the interval of interest may contribute significantly to the activity estimated within the interval, while some of the power carried by the structure inside the interval of interest falls outside and does not contribute to the spectral estimate.

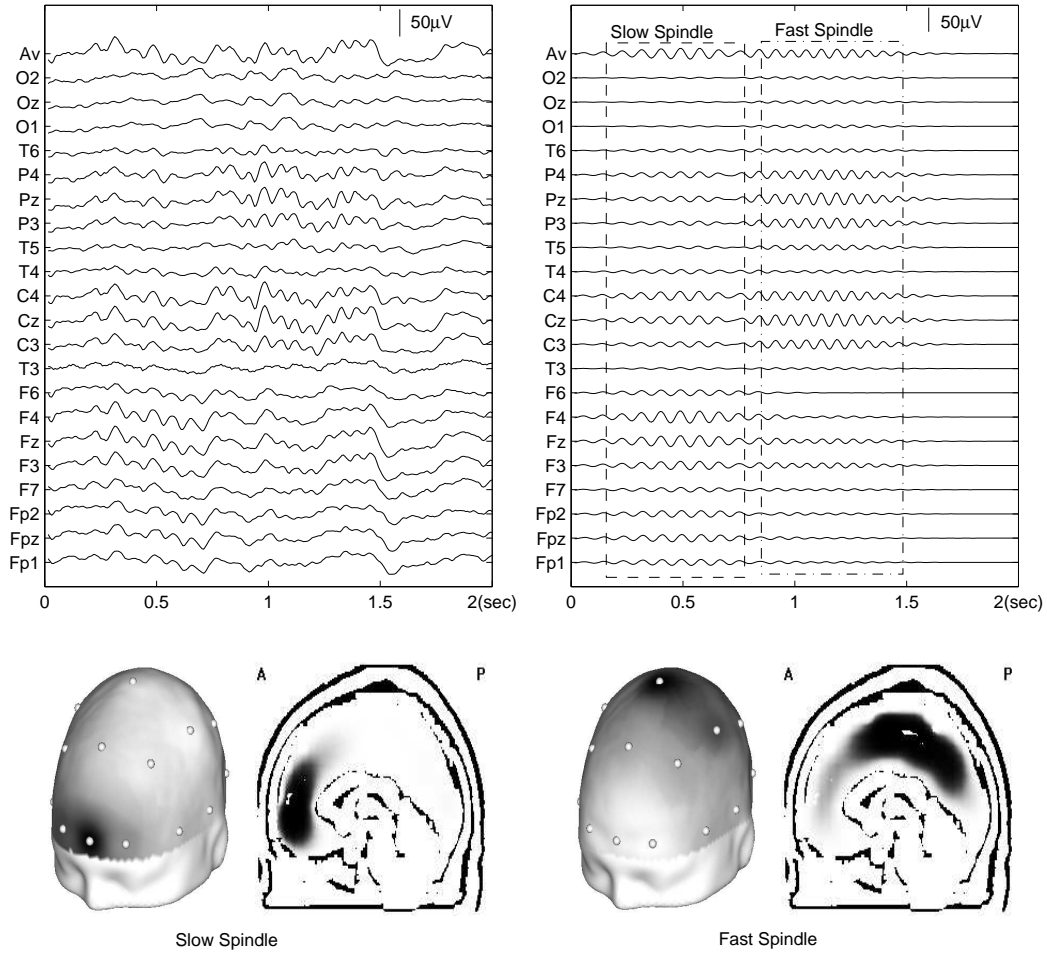


Fig. 2. Upper left: 2 seconds of sleep EEG from 21 standard electrodes (uppermost trace—average). Upper right: time courses of two Gabor atoms (Eq. (1)), conforming to the criteria of sleep spindles (section 2.3), fitted to the EEG presented on the left by the multichannel matching pursuit (section 2.1). The first atom (slow spindle) is centered around 0.5 s and 11 HZ. Center of second atom (fast spindle) is around 1 s and 14 Hz . Lower left: Topographic signature of the slow spindle, pronounced in the frontal derivations, and the corresponding Loreta image. Lower right: topographic signature of the fast spindle, pronounced in the parietal derivations, and the corresponding Loreta image.

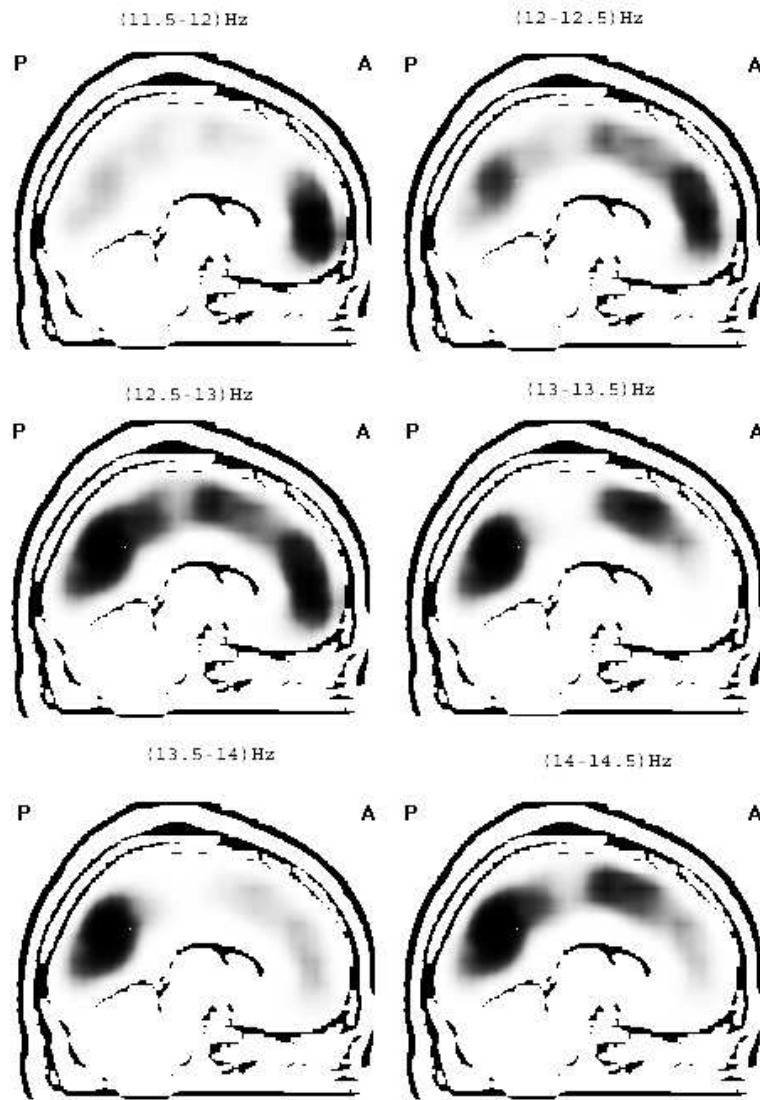


Fig. 3. Loreta images calculated for 6 single sleep spindles, chosen at random from the frequency intervals from 11.5–12 Hz (top left) to 14–14.5 Hz (bottom right). In each of these ranges one spindle was randomly chosen from the structures automatically detected and parameterized via the MMP. Corresponding panels present Loreta images computed for these single sleep spindles.

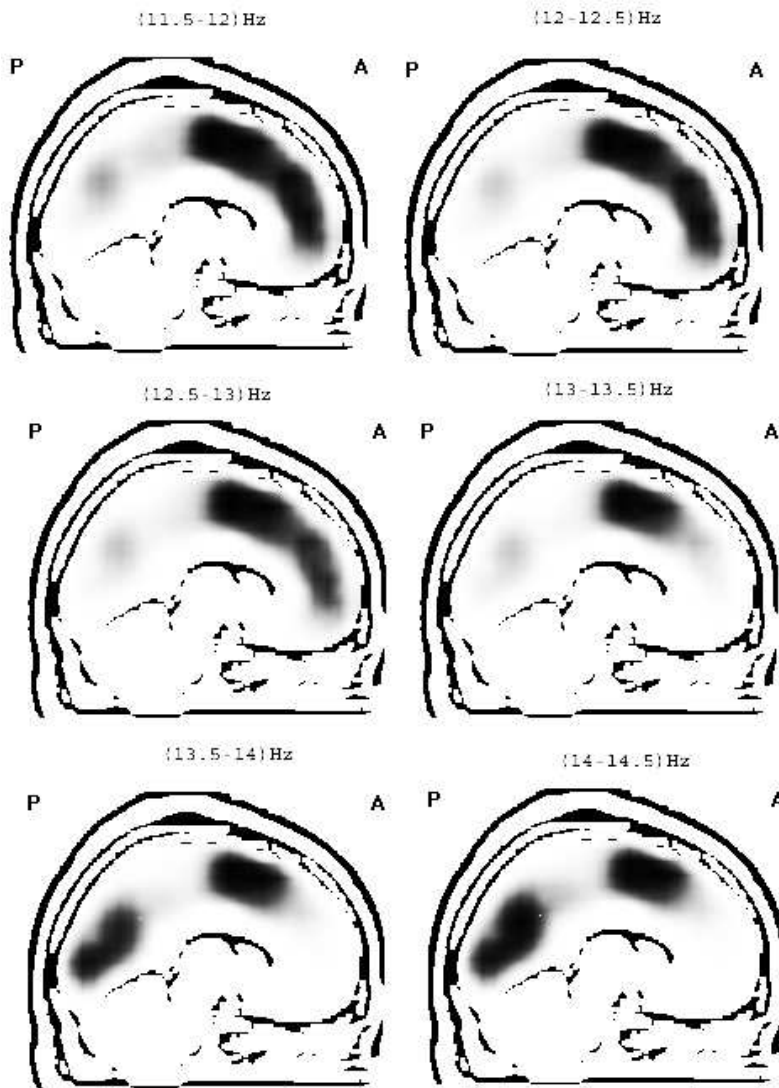


Fig. 4. Average Loreta images calculated for sleep spindles for the 5 recordings of subjects exhibiting clear prevalence of slow spindles in frontal regions. Separate averages constructed for spindles occurring in the frequency intervals from 11.5–12 Hz (top left) to 14–14.5 Hz (bottom right). No statistics or bias correction was employed in forming these images.

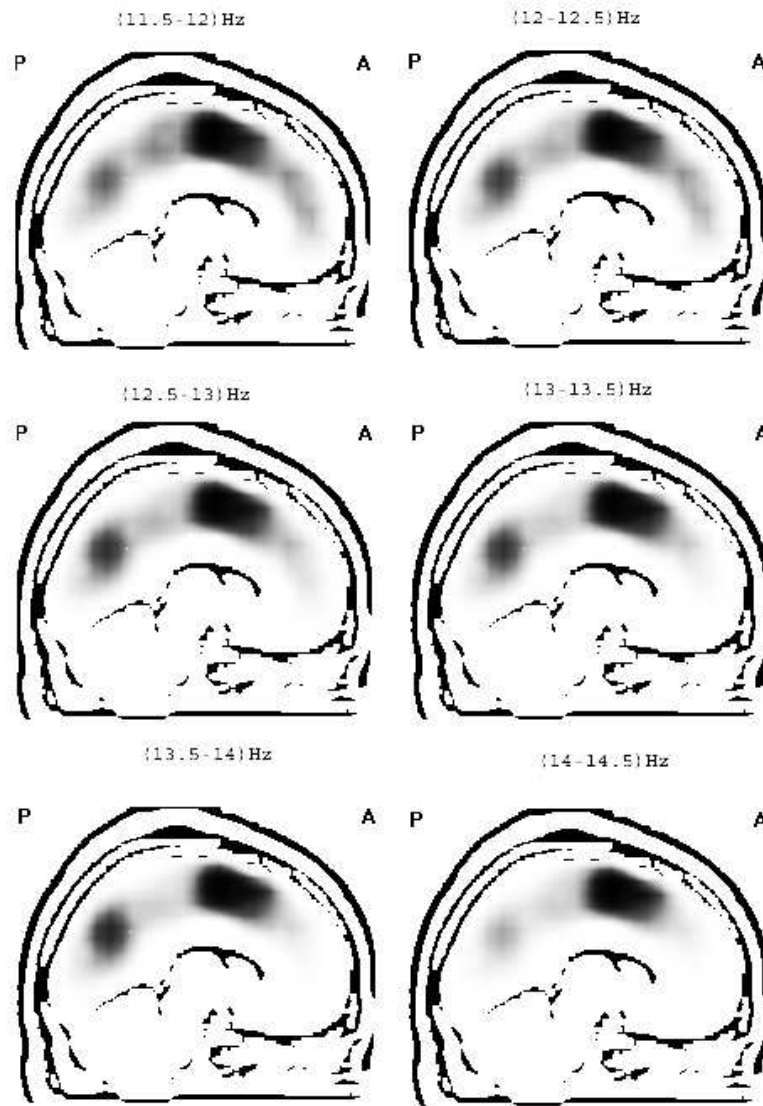


Fig. 5. The same as in Figure 4, averaged for the 15 recordings of subjects exhibiting “less clear” spatial distinction between fast and slow spindles.